A charge-decorated porous framework with polar pores and open O donor sites for CO_2/CH_4 and C_2H_2/C_2H_4 separations

Bin Tan,[a] Xing-Wu Liu,[b] Hao-Wang,[c] Guo-Yu Yang[a] and Jie Zhang*[a]

[a]MOE Key Laboratory of Cluster Science, Beijing Key Laboratory of Photoelectronic/Electrophotonic Conversion Materials, School of Chemistry and Chemical Engineering, Beijing Institute of Technology, Beijing 102488, P. R. China
E-mail: zhangjie68@bit.edu.cn

[b]Synfuels China Technology Co.Ltd., Beijing, 101407, P. R. China

[c]Hoffmann Institute of Advanced Materials, Shenzhen Polytechnic, 7098 Liuxian Boulevard, Nanshan District, Shenzhen 518055, P. R. China

Experiment Section

Materials and Methods. All reagents and chemicals were purchased from commercial sources and used without further purification. Powder X-ray diffraction (PXRD) patterns were recorded in the angular range of 2θ = 5-50° on a Miniflex II diffractometer using a Cu$K\alpha$ radiation. Thermogravimetric analysis (TGA) was carried out with a Mettler TGA/SDTA851^e thermal analyzer at a heating rate of 10 ℃·min^{-1} under an atmosphere of flowing air on the pure powder samples from 30 to 800 ℃. Gas adsorption measurement was performed in the ASAP (Accelerated Surface Area and Porosimetry) 2020 System. Vapor-phase adsorption isotherms were measured with an Intelligent Gravimetric Sorption Analyser IGA100B from the Hiden Corporation.

Synthesis of Zn-CP. The synthesis procedure can refer our previous work.[1] Typically, a mixture of 0.1 mmol pbpy·Cl_2 (0.049 g), 0.1 mmol H_4PMC (0.025 g), 2 mL $ZnSO_4$ solution (0.05 M) and 3 mL DMF stirred for 20 min, then sealed in a 20 mL vial and kept at 110 ℃ for 40 h. The yellow laminar-like crystals of Zn-CP were obtained.

The breakthrough measurements. The as-made sample was degassed at 110 ℃ for 5 hours in vacuum prior to measurements. Breakthrough experiments were executed by applying the separation column packed with the activated sample. For CO_2/CH_4

breakthrough experiments, were executed by applying with about 760 mg activated sample was packed into the separation column with the length of 10 cm and an internal diameter of 6 mm, while the helium with a rate of 10 mL (STP) min^{-1} kept flowing. The feed gases, binary CO_2/CH_4 (50/50, v/v) mixtures, were supplied to this measurement with a flow rate of 1 mL (STP) min^{-1} under 298 K and atmospheric pressure. The gas compositions at the outlet determined continuously by mass spectrometry (MS, MKS, CIRRUS-3). While for C_2H_2/C_2H_4 breakthrough experiments, 500 mg sample was filled in the column with the length of 8 cm and an internal diameter of 4 mm, while the helium kept flowing with a rate of 5 mL (STP) min^{-1}. The feed gases, binary C_2H_2/C_2H_4 (50/50, v/v) mixtures, were supplied to this measurement with a flow rate of 4 mL (STP) min^{-1} under 298 K and atmospheric pressure. The gas compositions at the outlet determined continuously by mass spectrometry (MS, Hiden, HPR-20).

Isosteric Heat of Adsorption

A virial type expression of the following form was used to fit the combined isotherm data for a given material at 273 and 298 K.[2]

$$\ln P = \ln N + 1/T \sum_{i=0}^{m} a_i N^i + \sum_{j=0}^{n} b_j N^j$$

Here, P is the pressure, N is the adsorbed amount, T is the temperature, a_i and b_j are virial coefficients, and m, n represents the number of coefficients required to adequately describe the isotherms. The values of the virial coefficients a_0 through a_m were then used to calculate the isosteric heat of adsorption.

The coverage-dependent isosteric heat of adsorption (Q_{st}):

$$Q_{st} = -R \sum_{i=0}^{m} a_i N^i$$

R is the universal gas constant, 8.314 $J \cdot mol^{-1} \cdot K^{-1}$.

Henry's law selectivity

To estimate reliable Henry's constants, a virial-type expression comprising the temperature-independent parameters a_i and b_j was applied:

$$\ln P = \ln N + 1/T \sum_{i=0}^{m} a_i N^i + \sum_{j=0}^{n} b_j N^j$$

Henry's constant (K_H):

$$K_H = exp(-b_0) \cdot exp(-a_0/T)$$

The Henry's law selectivity for gas component i over j is calculated based on:

$$S_{ij} = K_{Hi} / K_{Hj}$$

Adsorption selectivity base on IAST[3]

To better describe the single component adsorption isotherms, dual site Langmuir-Freundlich (DSLF) model was used and well-defined as:

$$q = A_1 \frac{b_1 p^{1/c_1}}{1 + b_1 p^{1/c_1}} + A_2 \frac{b_2 p^{1/c_2}}{1 + b_2 p^{1/c_2}}$$

Here, q (mmol/g) is the adsorbed amount, A_1 and A_2 (mmol/g) are the saturated capacities of site 1 and site 2, b_1 and b_2 (1/kPa) are the affinity coefficients to the sites 1 and 2, P (kPa) is the pressure, and c_1 and c_2 represent the deviations from an ideal homogeneous surface. The adsorption selectivities were established using IAST combined with DSLF to predict the selectivity of porous materials for binary gas.

The adsorption selectivity $S_{i,j}$ is defined as:

$$S_{ij} = \frac{x_i / x_j}{y_i / y_j}$$

Here, x_i and x_j are the gas uptake capacity at the adsorbed equilibrium of components i and j respectively. The gas molar fractions the i and j components are represented by y_i and y_j, respectively

Density-Functional Theory Calculations

All spin-polarized calculations were performed using VASP[4,5] with PAW method.[6,7] The exchange-correlation energy was treated using GGA-PBE function.[8] A cutoff energy of 400 eV was set for the plane-wave expansion. The convergence criteria for the force and electronic self-consistent iteration were set to 0.05 eV/Å and 10^{-4} eV, respectively. The bulk Zn-CP structure was fully relaxed. A Monkhorst-Pack method of k-points was used.[9] Binding energy of adsorbent (C_2H_2, C_2H_4, and CO_2) is defined as:

$$E_{binding} = E_{x/Zn-CP} - [E_{Zn-CP} + E_x]$$

Here, $E_{x/Zn-CP}$, E_{Zn-CP} and E_x are the total energy of the **Zn-CP** with adsorbents, the clean **Zn-CP** and the free adsorbent (x) in gas phase, respectively.

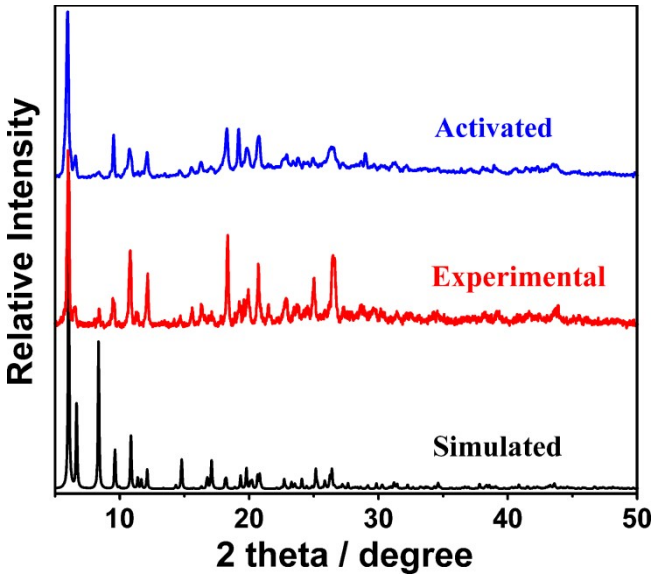

Fig. S1 PXRD patterns of **Zn-CP** before and after being activated.

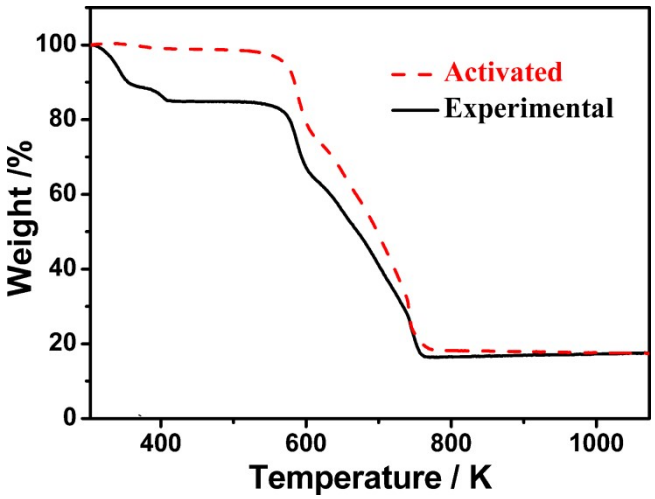

Fig. S2 TG curves for the as-synthesized **Zn-CP** and the activated sample.

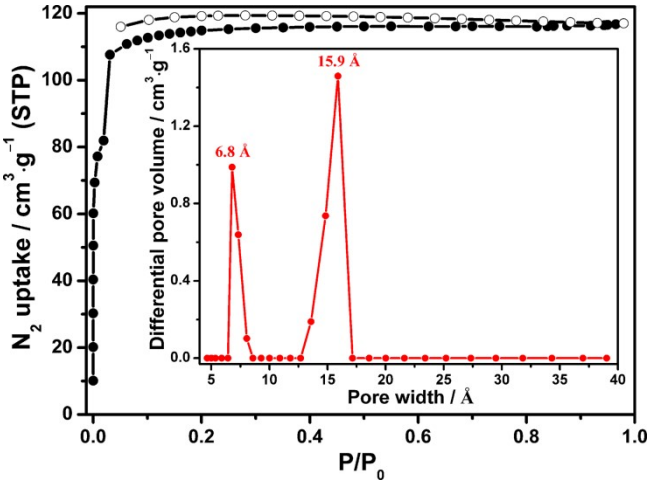

Fig. S3 N_2 adsorption (closed symbols) and desorption (open symbols) isotherms at 77 K. The inset shows the pore size distribution calculated by the DFT (density functional theory) method. STP stands for standard temperature and pressure.

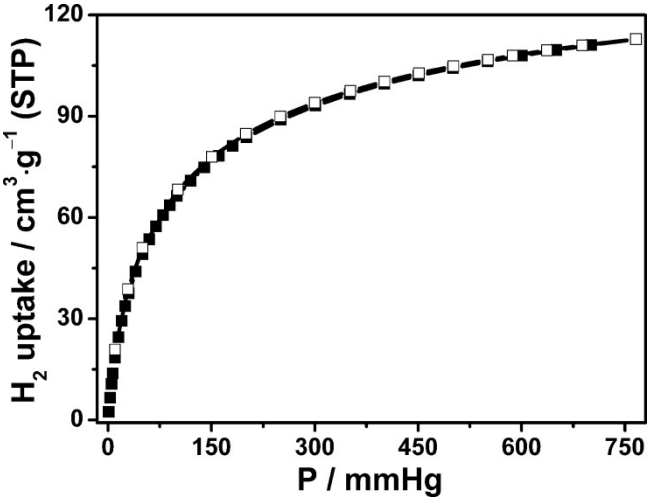

Fig. S4 H_2 adsorption (closed symbols) and desorption (open symbols) isotherms at 77 K.

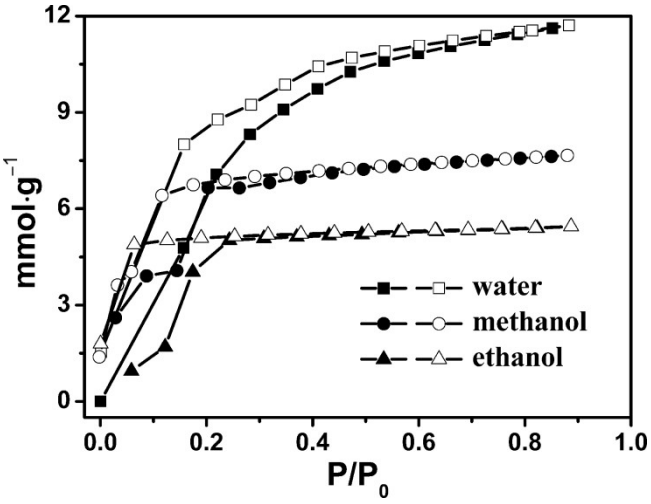

Fig. S5 The vapor adsorption (closed symbols) and desorption (open symbols) isotherms.

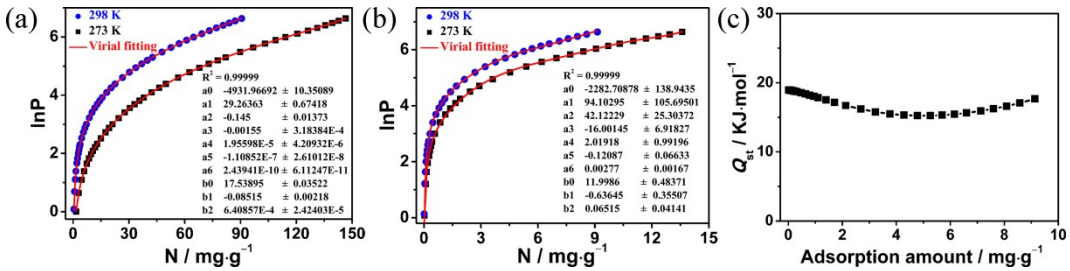

Fig. S6 Fitted CO_2 (a) and CH_4 (b) adsorption isotherms; (c) isosteric heat of CH_4 adsorption.

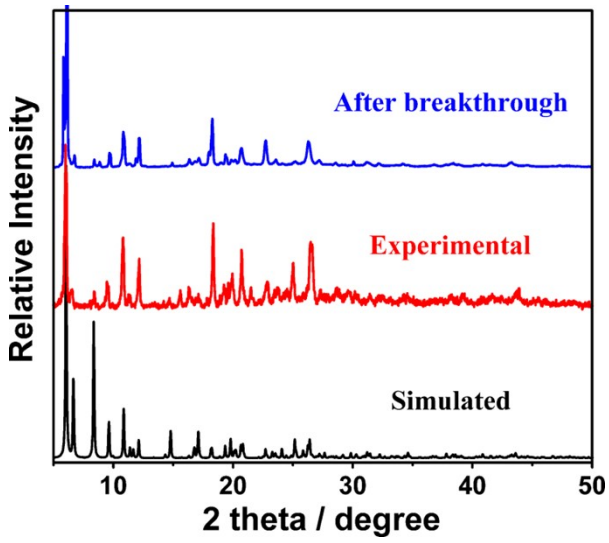

Fig. S7 PXRD patterns of **Zn-CP** before and after the CO_2/CH_4 (50/50, v/v) breakthrough experiments.

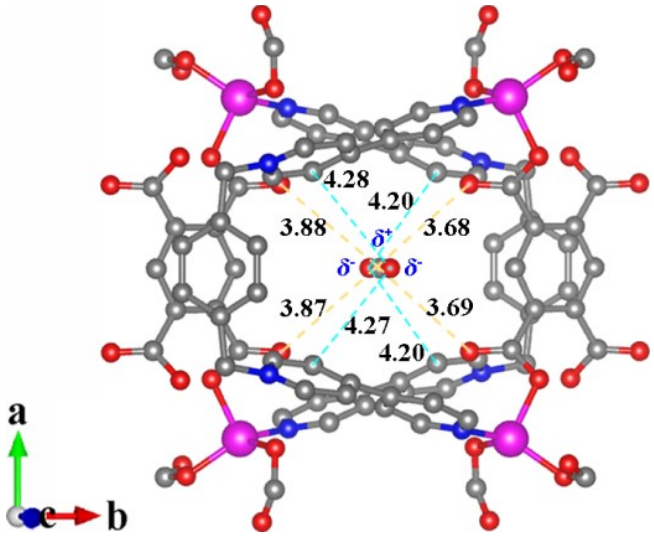

Fig. S8 DFT optimized geometry for CO_2 located in the channel of **Zn-CP** ($E_{binding}$ = -1.16 eV). Close contact distances (in Å) are marked. Magenta, gray, blue and red represent Zn, C, N and O atoms, respectively.

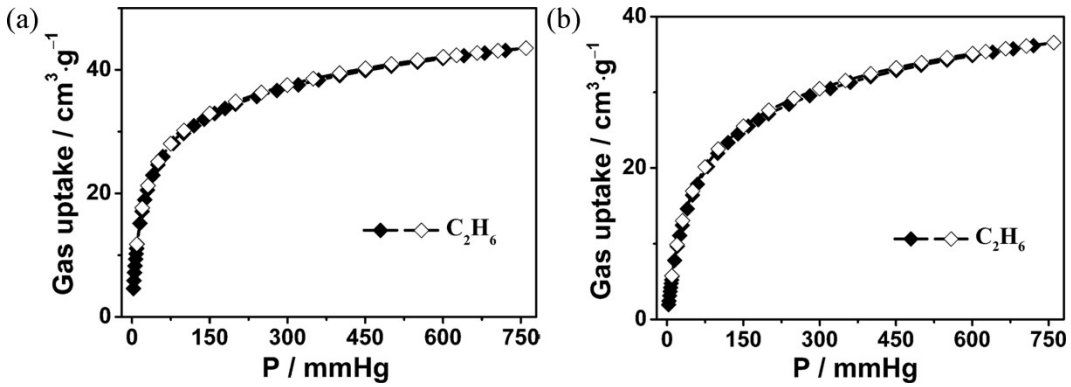

Fig. S9 C_2H_6 adsorption (closed symbols) and desorption (open symbols) isotherms at 273 K (a) and 297 K (b), respectively.

Under 1 bar, the maximum uptakes of C_2H_6 are 43.5 and 36.6 $cm^3 \cdot g^{-1}$ measured at 273 K and 298 K, respectively.

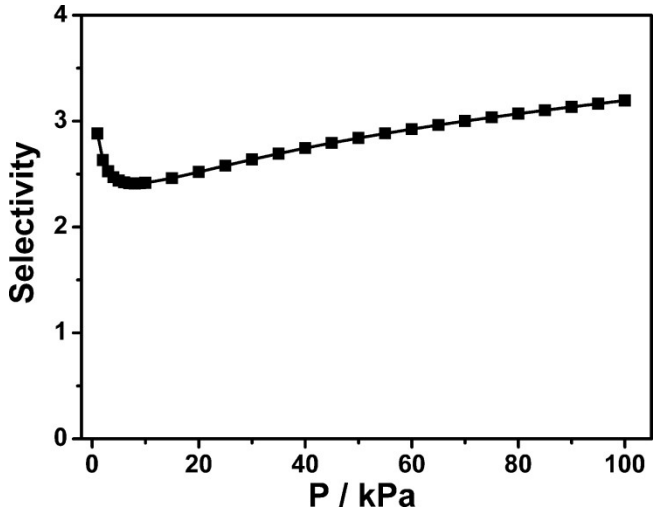

Fig. S10 IAST predicted C_2H_2/C_2H_4 (50/50, v/v) selectivity at 298 K.

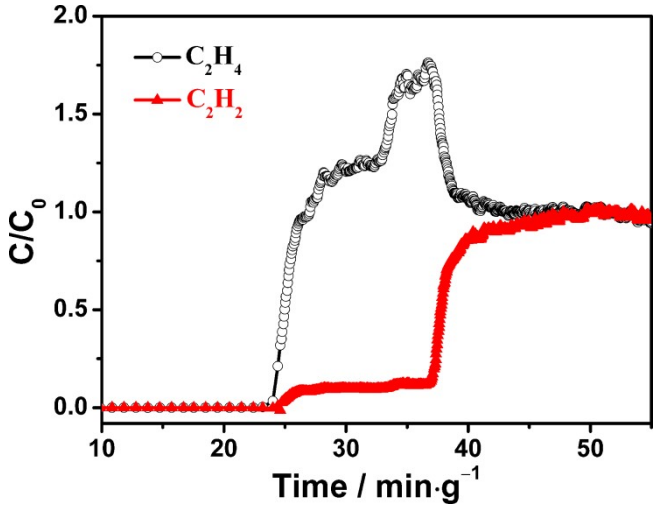

Fig. S11 Experimental column breakthrough curves for C_2H_2/C_2H_4 (50/50, v/v) separation with **Zn-CP** at 298 K and 1 bar.

The breakthrough curves present a ‘‘roll-up’’ before C_2H_4 breakthrough occurs completely, indicating that the flow rate temporarily exceeds the feed flow rate. For **Zn-CP**, the roll-up might be attributed to the desorption of C_2H_4 within the pore structures induced by C_2H_2.[10]

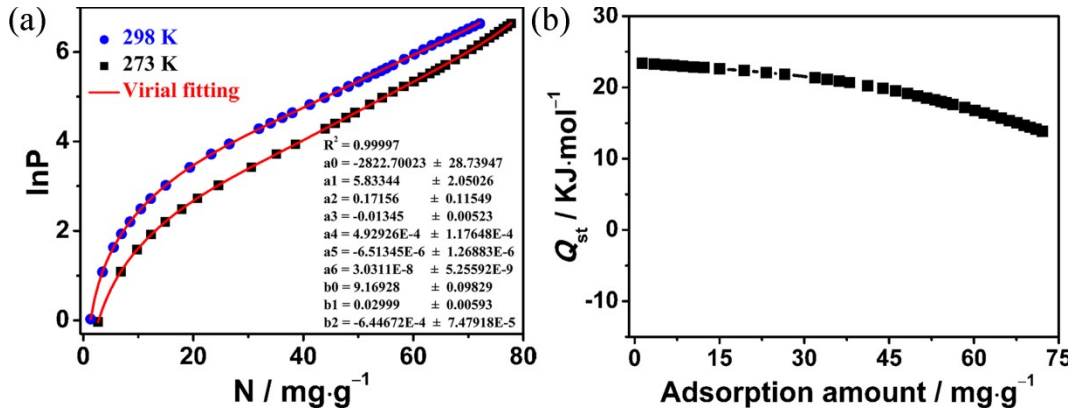

Fig. S12 (a) Fitted C_2H_2 adsorption isotherms; (b) isosteric heat of C_2H_2 adsorption.

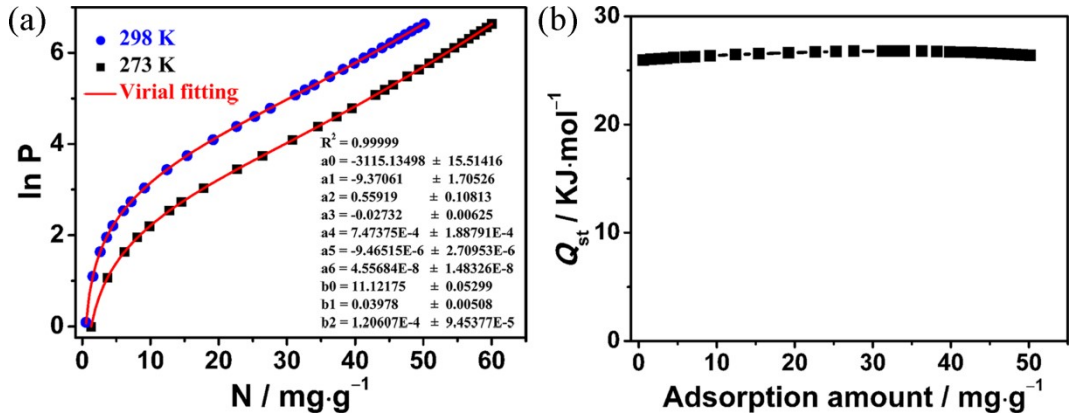

Fig. S13 (a) Fitted C_2H_4 adsorption isotherms; (b) isosteric heat of C_2H_4 adsorption.

The Q_{st} values of C_2H_2 and C_2H_4 at zero coverage are calculated to be 23.4 and 25.9 kJ·mol^{-1}, respectively (Figs. S12-13). The C_2H_2 Q_{st} value is comparable to those of the reported CPs with functional amine groups UTSA-100a (22 kJ·mol^{-1}),[11] cyclodextrin-based CD-MOF-2 (25.8 kJ·mol^{-1})[12] and M′MOF-3a (27.3 kJ·mol^{-1}).[13] The relatively low adsorption heat facilitates for the regeneration of C_2H_2 from **Zn-CP** by avoiding the high energy consumption. Although the adsorption heat of C_2H_2 was slightly lower than that of C_2H_4, due to the pore environment to form the distinct intermolecular H-bond interaction, **Zn-CP** exhibits higher uptake for C_2H_2 over C_2H_4.[14]

Table S1. CO_2/CH_4 separation selectivities calculated by Henry's law and IAST methods at 298 K.

Adsorbate	Henry's law selectivity			IAST selectivity (1 atm)	
	K_H	a_0	b_0	S_{ij}*	S_{ij}
CO_2	0.37	-4932±10	17.54±0.035	/	/
CH_4	0.013	-2283±139	11.99±0.48	28.5	8.8

* The Henry's law selectivities S_{ij} * for gas component CO_2 over CH_4 at the speculated temperatures are calculated based on equation: $S_{ij}* = K_H(CO_2)/K_H(CH_4)$.

Table S2. Summary of the adsorption data for C_2H_2 and C_2H_4 in various PCPs.

CPs	S_{BET} ($m^2 \cdot g^{-1}$)[a]	C_2H_2 uptake ($mmol \cdot g^{-1}$)	C_2H_4 uptake ($mmol \cdot g^{-1}$)	C_2H_2/C_2H_4 uptake ratio[f]	IAST selectivity	*Ref*
FeMOF-74	1350	6.8[c]	6.1[c]	1.11	1.87	15,16
MgMOF-74	927	8.37[d]	7.45[d]	1.12	2.18	15,16
CoMOF-74	1018	8.17	7.02	1.16	1.70	15,16
ZJNU-14	883	4.00	3.25	1.23	1.63	17
Ni-DCPTP	857	6.54	4.48	1.46	5.5	18
NOTT-300	1370	6.34[e]	4.28[e]	1.48	2.30	19
Zn-CP	**367**	**2.77**	**1.79**	**1.55**	**3.20**	**This work**
CPL-5	523[b]	3.01	1.84	1.64	5.99	20

Summary of the adsorption data were collected at 298 K. [a]S_{BET} (Brunauer-Emmett-Teller specific surface area) calculated from N_2 isotherms at 77 K. [b]S_{BET} calculated from CO_2 isotherms at 195~196 K. [c]318 K. [d]296 K. [e]293 K. [f]For ratios of the total uptake capacities at 1 bar.

References

1 B. Tan, C. Chen, L. X. Cai, Y. J. Zhang, X. Y. Huang and J. Zhang, Introduction of Lewis Acidic and Redox-Active Sites into a Porous Framework for Ammonia Capture with Visual Color Response, *Inorg. Chem.*, 2015, **54**, 3456-3461.

2 J. L. C. Rowsell and O. M. Yaghi, Effects of Functionalization, Catenation, and Variation of the Metal Oxide and Organic Linking Units on the Low-Pressure Hydrogen Adsorption Properties of Metal-Organic Frameworks, *J. Am. Chem. Soc.*, 2006, **128**, 1304-1315.

3 A. L. Myers and J. M. Prausnitz, Thermodynamics of mixed-gas adsorption, *AIChE J.*, 1965, **11**, 121-127.

4 G. Kresse and J. Furthmüller, Efficiency of ab-initio total energy calculations for metals and semiconductors using a plane-wave basis set, *Comp. Mater. Sci.*, 1996, **6**, 15-50.
5 G. Kresse and J. Furthmüller, Efficient iterative schemes for *ab initio* total-energy calculations using a plane-wave basis set, *Phys. Rev. B*, 1996, **54**, 11169-11186.
6 P. E. Blöchl, Projector augmented-wave method, *Phys. Rev. B*, 1994, **50**, 17953-17979.
7 G. Kresse and D. Joubert, From ultrasoft pseudopotentials to the projector augmented-wave method, *Phys. Rev. B*, 1999, **59**, 1758-1775.
8 J. P. Perdew, K. Burke and M. Ernzerhof, Generalized Gradient Approximation Made Simple, *Phys. Rev. Lett.*, 1996, **77**, 3865-3868.
9 H. J. Monkhorst and J. D. Pack, Special points for Brillouin-zone integrations, *Phys. Rev. B*, 1976, **13**, 5188-5192.
10 P.-D. Zhang, X.-Q. Wu, T. He, L.-H. Xie, Q. Chen and J.-R. Li, Selective adsorption and separation of C_2 hydrocarbons in a "flexible-robust" metal-organic framework based on a guest-dependent gate-opening effect, *Chem. Commun.*, 2020, **56**, 5520-5523.
11 T.-L. Hu, H. L. Wang, B. Li, R. Krishna, H. Wu, W. Zhou, Y. F. Zhao, Y. Han, X. Wang, W. D. Zhu, Z. Z. Yao, S. C. Xiang and B. L. Chen, Microporous metal-organic framework with dual functionalities for highly efficient removal of acetylene from ethylene/acetylene mixtures, *Nat. Commun.*, 2015, **6**, 7328.
12 L. Y. Li, J. W. Wang, Z. G. Zhang, Q. W. Yang, Y. W. Yang, B. G. Su, Z. B. Bao and Q. L. Ren, Inverse Adsorption Separation of CO_2/C_2H_2 Mixture in Cyclodextrin-Based Metal-Organic Frameworks, *ACS Appl. Mater. Interfaces*, 2019, **11**, 2543-2550.
13 S.-C. Xiang, Z. J. Zhang, C.-G. Zhao, K. L. Hong, X. B. Zhao, D.-R. Ding, M.-H. Xie, C.-D. Wu, M. C. Das, R. Gill, K. M. Thomas and B. L. Chen, Rationally tuned micropores within enantiopure metal-organic frameworks for highly selective separation of acetylene and ethylene, *Nat. Commun.*, 2011, **2**, 204.
14 X. L. Cui, K. J. Chen, H. B. Xing, Q. W. Yang, R. Krishna, Z. B. Bao, H. Wu, W. Zhou, X. L. Dong, Y. Han, B. Li, Q. L. Ren, M. J. Zaworotko and B. L. Chen, Pore chemistry and size control in hybrid porous materials for acetylene capture from ethylene, *Science*, 2016, **353**, 141-144.
15 E. D. Bloch, W. L. Queen, R. Krishna, J. M. Zadrozny, C. M. Brown and J. R. Long, Hydrocarbon Separations in a Metal-Organic Framework with Open Iron(II) Coordination Sites, *Science*, 2012, **335**, 1606-1610.
16 S. J. Geier, J. A. Mason, E. D. Bloch, W. L. Queen, M. R. Hudson, C. M. Browncd and J. R. Long, Selective adsorption of ethylene over ethane and propylene over propane in the metal-organic frameworks M_2(dobdc) (M = Mg, Mn, Fe, Co, Ni, Zn), *Chem. Sci.*, 2013, **4**, 2054-2061.
17 Z. Z. Jiang L. H. Fan P. Zhou T. T. Xu J. X. Chen S. M. Hu, D.-L. Chen and Y. B. He, An N-oxide-functionalized nanocage-based copper-tricarboxylate framework for the selective capture of C_2H_2, *Dalton Trans.*, 2020, **49**, 15672-15281.
18 H.-H. Wang, Q.-Y. Liu, L. B. Li, R. Krishna, Y.-L. Wang, X.-W. Peng, C.-T. He, R.-B. Lin and B. L. Chen, Nickel-4′-(3,5-dicarboxyphenyl)-2,2′,6′,2″-terpyridine Framework: Efficient Separation of Ethylene from Acetylene/Ethylene Mixtures with a High Productivity, *Inorg. Chem.*, 2018, **57**, 9489-9494.
19 S. H. Yang, A. J. Ramirez-Cuesta, R. Newby, V. Garcia-Sakai, P. Manuel, S. K. Callear, S. I. Campbell, C. C. Tang and M. Schröder, Supramolecular binding and separation of hydrocarbons within a functionalized porous metal-organic framework, *Nat. Chem.*, 2015, **7**, 121-129.
20 F. Zheng, L. D. Guo, B. X. Gao, L. Y. Li, Z. G. Zhang, Q. W. Yang, Y. W. Yang, B. G. Su, Q. L. Ren and Z. B. Bao, Engineering the Pore Size of Pillared-Layer Coordination Polymers Enables Highly Efficient Adsorption Separation of Acetylene from Ethylene, *ACS Appl. Mater. Interfaces*, 2019, **11**, 28197-28204.